INTERNATIONAL JOURNAL FOR NUMERICAL METHODS IN FLUIDS
Int. J. Numer. Meth. Fluids 2011; **65**:683–698
Published online 22 December 2009 in Wiley Online Library (wileyonlinelibrary.com). DOI: 10.1002/fld.2210

Reduction in drag and vortex shedding frequency through porous sheath around a circular cylinder

S. Bhattacharyya[1,*,†] and A. K. Singh[1,2]

[1]*Department of Mathematics, Indian Institute of Technology, Kharagpur 721302, India*
[2]*Helmholtz Center for Environmental Research—UFZ, Leipzig 04318, Germany*

SUMMARY

A numerical study on the laminar vortex shedding and wake flow due to a porous-wrapped solid circular cylinder has been made in this paper. The cylinder is horizontally placed, and is subjected to a uniform cross flow. The aim is to control the vortex shedding and drag force through a thin porous wrapper around a solid cylinder. The flow field is investigated for a wide range of Reynolds number in the laminar regime. The flow in the porous zone is governed by the Darcy–Brinkman–Forchheimer extended model and the Navier–Stokes equations in the fluid region. A control volume approach is adopted for computation of the governing equations along with a second-order upwind scheme, which is used to discretize the convective terms inside the fluid region. The inclusion of a thin porous wrapper produces a significant reduction in drag and damps the oscillation compared with a solid cylinder. Dependence of Strouhal number and drag coefficient on porous layer thickness at different Reynolds number is analyzed. The dependence of Strouhal number and drag on the permeability of the medium is also examined. Copyright © 2009 John Wiley & Sons, Ltd.

Received 13 November 2008; Revised 9 August 2009; Accepted 19 September 2009

KEY WORDS: fluid–porous interface; vortex shedding; passive control; pressure correction; upwind difference

1. INTRODUCTION

The unsteady flow around bluff bodies has been studied extensively over the years because of its use in numerous engineering applications. The vortex shedding from the cylinder leads to a large fluctuation in pressure forces in a direction transverse to the flow, which in turn produces structural vibration, acoustic noise, or resonance. The flow control aims to reduce the resistance and the magnitude of the fluctuating force acting on the body. An effective flow control may save energy, increase propulsion efficiency, and also reduce the vibration of the body.

There have been numerous investigations in the past aiming to alter or suppress the pattern of vortex shedding. In general, flow control techniques for reducing the aerodynamic drag exerted on a bluff body are classified into two types: active and passive control techniques. Active control methods control the flow by supplying external energy through several means such as rotational oscillatory motion of the bluff body or jet blowing. Because of this, active control techniques require complex mechanical devices that supply external power to the flow. Passive control techniques control the vortex shedding by modifying the shape of the bluff body [1] or by attaching additional

*Correspondence to: S. Bhattacharyya, Department of Mathematics, Indian Institute of Technology, Kharagpur 721302, India.
†E-mail: somnath@maths.iitkgp.ernet.in

Contract/grant sponsor: Council of Scientific & Industrial Research.

devices in the flow stream. Therefore, the passive control technique is energy free and often easier to implement.

Among the passive control techniques, the splitter plate has been considered as one of the most successful devices to control the vortex shedding behind a cylinder [1]. Subsequently, several authors namely Ozono [2, 3] and Hwang *et al.* [4] have studied the control of vortex shedding and drag reduction through the splitter plate. Another approach of controlling the flow behind a bluff body is to place a smaller bluff body in tandem with the main body. The reattachment of shear layers emerging from the front bluff body with the main body causes a substantial drag reduction and damping in oscillation. Nakamura and Igarashi [6] have discussed the passive control of vortex shedding by attaching a ring around the cylinder.

A porous layer separating the solid body and the fluid may reduce the shear stress experienced by the body. Besides, the use of porous wrapper on solid structure has also applications in heat transfer technology [7]. Vafai and Kim [8] found that the porous substrate, which is underlying a fluid layer, causes a blowing effect on the flow field resulting in a significant reduction in the frictional drag. The introduction of a porous sheath reduces the vorticity production as it diffuses both outer and inner layers of the porous–fluid interface. Therefore, it is expected that a thin porous coating around the cylinder may create a significant impact on vortex shedding and surface force. Porous layers have also been used for passive control in shock wave–boundary layer interactions [9].

The passive control of vortex shedding from a cylinder using a porous sheath has been recently investigated by Bruneau and Mortazavi [10–13]. Such a type of control involves separation of the solid surface from the fluid by a porous interface. Therefore, they considered the passive control of the two-dimensional flow around circular/square cylinders and square back Ahmed bodies. This passive control method yields a drastic regularization of the flow for high Reynolds numbers. They found that by adding a porous ring around a riser pipe section, the vortex-induced vibrations can be substantially reduced. However, they confined their analysis for a particular value of the porous layer thickness in the turbulent range of Reynolds number. Sobera *et al.* [14] made a study on the flow at sub-critical Reynolds number around a circular cylinder surrounded at some fixed small distance by a porous layer. All those studies involving porous layers were made for certain fixed values of Reynolds number in the transitional or turbulent range where the flow is relatively insensitive to Reynolds number. The effect of Reynolds number on vortex shedding and surface forces experienced by the bluff body have not been determined.

Fluid flow modeling of configurations involving fluid–porous–solid interfaces is a challenge. This involves the study of fluid flow above and through a porous medium. The flow over the fluid region is governed by the Navier–Stokes equation, and the flow through the porous medium is governed by the generalized momentum equation, which includes the effects of flow inertia as well as friction caused by macroscopic shear stress. Darcy's law is the oldest model used to describe the flow of fluid through a porous media. It represents a force balance between the pressure gradient and the resistance applied by the medium. As the Darcy equation has no associated stress tensor, special care is needed for the boundary condition along the interface. Several forms of the boundary conditions have been discussed in the book by Ingham and Pop [15]. The Brinkman equation has the advantage that it contains the stress tensor, thus the boundary condition is the continuity assumption of momentum and viscous stress along the porous–solid interface boundary. Nazar *et al.* [16] studied the boundary layer flow past a circular cylinder in a porous medium through the Brinkman model. Khanafer *et al.* [17] employed the extended Brinkman–Darcy's law to describe the flow motion inside the porous sleeve.

It has been proved by both theoretical evaluation and experimentation that Darcy's law is not appropriate for strong flow through porous bodies. The influence of inertial forces on the flow behavior in highly porous structures is studied by Costa *et al.* [18]. They have shown that the Forchheimer model remains valid for sufficiently high Reynolds number, even when convective non-linearities can significantly affect the momentum transport at the pore scale. Fourar *et al.* [19] show that there is a critical value of the Reynolds number depending on the flow dimensions from which Darcy's law is no longer valid. They also observed that the Forchheimer model is a good approximation for describing flow at high Re, i.e. in the non-Darcy flow regime.

DOI: 10.1002/fld

To simulate the composite systems of fluid and porous media, it is necessary to simultaneously solve the Brinkman equation in the porous media and the Navier–Stokes equation in the clear fluids along with a suitable matching condition at the interface. The implementation of the interface condition [20, 21] is complicated as it contains material-dependent parameters whose value must be determined empirically. In the single-domain formulation [7], the two sets of equations for the fluid and the porous regions are combined into one set by introducing a binary parameter.

The objectives of the present study are to numerically investigate the characteristics of the two-dimensional laminar flow over a porous sheath solid cylinder, and then to make a qualitative and quantitative comparison with the wake flow due to a solid cylinder. The underlying mechanism for controlling the wake through the porous layer has been analyzed in the present paper. We investigate the effect of porous wrapper for a wide range of Re at different values of thickness and permeability of the porous layer. It has been reported that a two-dimensional flow field past a solid circular cylinder is observed until the Reynolds number reaches a critical value, which is around 194 [22]. Beyond this Reynolds number, the oblique vortex shedding mode, i.e. type-A and type-B instability sets in and, subsequently, a turbulent flow develops. It is expected that for relatively low permeability, the main characteristics of the flow around the porous sheath solid cylinder is very similar to those of the flow around a solid cylinder at the same Reynolds number. We have confined our study in the parallel vortex shedding regime. However, as pointed out by Hammache and Gharib [23], parallel vortex shedding over the whole span can be induced with the help of some end-modification methods. Besides, the two-dimensional patterns of vortex shedding from a bluff body have the same qualitative features of the fully developed turbulent phase-averaged results [24]. It may be noted that the previous studies reported on this topic [10–13] considered certain discrete values of Re in the transitional and turbulent range, and restricted to a two-dimensional analysis. In the turbulent range of Reynolds number, the Darcy–Brinkman model becomes questionable due to the inertial fluctuation of the velocity field in the porous zone.

2. GOVERNING EQUATION

We consider that a porous-wrapped solid cylinder is horizontally placed (Figure 1) and is subjected to a uniform cross flow U_∞. The porous layer has a uniform porosity ε and permeability k. The radius of the cylinder R and free-stream velocity U_∞ are taken to be the characteristic length and velocity scale, respectively.

The governing equations in the fluid domain are the Navier–Stokes equations whereas the Darcy–Brinkman–Forchheimer extended model is used to describe the flow in the porous layer.

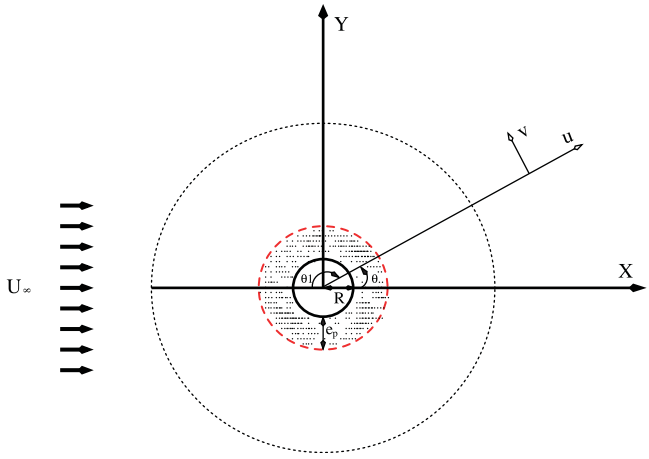

Figure 1. Sketch of the flow configuration.

DOI: 10.1002/fld

As the present configuration involves porous–solid and fluid–porous interfaces, the Brinkman model is used to account for the jump in shear stress. At moderate values of Reynolds number, the non-Darcy flow may occur in the porous region. The inertial forces in this range of Reynolds number may distort the flow lines. The non-linear inertial effect can be expressed through the quadratic Forchheimer term. We use the Dupuit–Forchheimer relationship [25], i.e. the volume-averaged fluid velocity $\mathbf{q}$ is related to the intrinsic (average over the fluid volume only) velocity $\mathbf{V}$ by $\mathbf{q}=\varepsilon\mathbf{V}$. Thus, the generalized Navier–Stokes equations can be expressed as:

$$\nabla\cdot\mathbf{q}=0, \tag{1}$$

$$\frac{1}{\varepsilon}\frac{\partial\mathbf{q}}{\partial t}+\frac{1}{\varepsilon^2}(\mathbf{q}\cdot\nabla)\mathbf{q}=-\frac{1}{\rho}\nabla p-\frac{v_e}{\mathbf{k}}\mathbf{q}+v_e\nabla^2\mathbf{q}-\frac{c_F}{\sqrt{\mathbf{k}}}|\mathbf{q}|\mathbf{q}, \tag{2}$$

where v_e is the effective viscosity and ρ is the fluid density. The form of the Forchheimer term (second term in the r.h.s. of Equation (1)) is suggested by Vafai [26].

We adopt a unified single-domain approach ([7, 27] and the references therein). In this approach, the two sets of equations for the fluid and the porous regions are combined into one set using appropriate switching terms. When this single set of equations is integrated over control volumes, it automatically takes care of the interfacial conditions. Thus, the present approach does away with the need for separate interface conditions. The equations governing the unsteady laminar flow through and around the porous layer in the non-dimensional form can be expressed as:

$$\frac{1}{r}\frac{\partial(ru)}{\partial r}+\frac{1}{r}\frac{\partial v}{\partial\theta}=0, \tag{3}$$

$$\begin{aligned}&\frac{1}{\varepsilon}\frac{\partial u}{\partial t}+\frac{1}{\varepsilon^2}\left(\frac{v}{r}\frac{\partial u}{\partial\theta}+u\frac{\partial u}{\partial r}-\frac{v^2}{r}\right)\\&\quad=-\frac{\partial p}{\partial r}+\frac{2}{Re}\left(\frac{\partial^2 u}{\partial r^2}+\frac{1}{r}\frac{\partial u}{\partial r}+\frac{1}{r^2}\frac{\partial^2 u}{\partial\theta^2}-\frac{2}{r^2}\frac{\partial v}{\partial\theta}-\frac{u}{r^2}\right)-\frac{2B}{ReDa}u-\frac{B1.75}{\sqrt{150}}\frac{1}{Da}\frac{\sqrt{u^2+v^2}}{\varepsilon^{3/2}}u,\end{aligned} \tag{4}$$

$$\begin{aligned}&\frac{1}{\varepsilon}\frac{\partial v}{\partial t}+\frac{1}{\varepsilon^2}\left(\frac{v}{r}\frac{\partial v}{\partial\theta}+u\frac{\partial v}{\partial r}-\frac{uv}{r}\right)\\&\quad=-\frac{1}{r}\frac{\partial p}{\partial\theta}+\frac{2}{Re}\left(\frac{\partial^2 v}{\partial r^2}+\frac{1}{r}\frac{\partial v}{\partial r}+\frac{1}{r^2}\frac{\partial^2 v}{\partial\theta^2}+\frac{2}{r^2}\frac{\partial u}{\partial\theta}-\frac{v}{r^2}\right)-\frac{2B}{ReDa}v-\frac{B1.75}{\sqrt{150}}\frac{1}{Da}\frac{\sqrt{u^2+v^2}}{\varepsilon^{3/2}}v.\end{aligned} \tag{5}$$

In the clear fluid region, the Darcy number tends to infinity with $\varepsilon=1$. The binary parameter $B=0$ in clear fluid region and $B=1$ in porous zone.

The dimensionless variable are defined as:

$$u=\frac{u^*}{U_\infty},\quad v=\frac{v^*}{U_\infty},\quad t=\frac{U_\infty t^*}{R},\quad p=\frac{p^*}{\rho U_\infty^2}. \tag{6}$$

The variable with superscript $(*)$ denotes dimensional variables. Here u, v, and p denote the radial velocity component, the cross-radial velocity component, and pressure. The dimensionless governing parameters are Reynolds number $Re=2RU_\infty/v$ and Darcy number $Da=k/R^2$. The non-dimensional thickness of the porous layer is denoted by e_p. The viscosity ratio is considered to be 1 in the present case.

We imposed no-slip condition on the surface of the solid cylinder ($r=1$). The upstream boundary condition is due to the uniform stream and a symmetry condition is assumed on the far downstream of the cylinder. It may be noted that in the present formulation, no boundary condition is required at the fluid–porous interface.

DOI: 10.1002/fld

The surface pressure coefficients C_p and C_{pi} along the solid surface and fluid–porous interface are defined, respectively as

$$C_p = \frac{(p_s^* - p_\infty^*)}{0.5\rho U_\infty^2}, \quad C_{pi} = \frac{(p_i^* - p_\infty^*)}{0.5\rho U_\infty^2}. \tag{7}$$

The subscripts i, s, and ∞ denote that the quantity is measured on the interface, solid surface, or far-field, respectively.

The Strouhal number (St) is a measure of the non-dimensional frequency of vortex shedding in the wake region and defined as:

$$St = \frac{fR}{U_\infty}, \tag{8}$$

where f is the vortex shedding frequency.

3. NUMERICAL METHOD

The governing equations are discretized through the finite volume method. This method involves integrating the continuity and momentum equations over a two-dimensional control volume on a staggered grid [28]. In the staggered grid system, the pressure is evaluated at each cell center and the velocity components are evaluated at the midpoints of the cell sides to which they are normal. Different control volumes are used to integrate different equations. Figure 2(a),(b) shows the control volume for continuity and u-momentum equation. The control volume formulation ensures conservation of momentum as well as continuity of fluxes. In the single-domain approach, as adopted here, the values from both sides of the interface are used to obtain solutions, and therefore the matching of variable values is inherent.

To discretize the momentum equations, the convective terms at the interface of each control volumes are estimated by a liner extrapolation between the values of the variables at two upwind neighbors. This ensures numerical stability at higher values of Reynolds number.

The u-momentum equation after integration over the u-control volume (Figure 2(a)) becomes

$$\frac{r\delta r\delta\theta}{\delta t}(u_p^{n+1} - u_p^n) + F_e u_e^{n+1} - F_w u_w^{n+1} + F_n u_n^{n+1} - F_s u_s^{n+1} = b. \tag{9}$$

where F_e is the nonlinear coefficient of u_e and b contains the source and diffusion terms. The variable u_e is estimated through a quadratic interpolation or extrapolation as explained below.

$$u_e = \frac{3}{8}u_E + \frac{3}{4}u_P - \frac{1}{8}u_W \quad \text{if } F_e > 0$$

$$u_e = \frac{3}{4}u_E + \frac{3}{8}u_P - \frac{1}{8}u_{EE} \quad \text{if } F_e < 0$$

Thus, we can express

$$F_e u_e = \left(\frac{3}{8}u_E + \frac{3}{4}u_P - \frac{1}{8}u_W\right)[[F_e, 0]] - \left(\frac{3}{4}u_E + \frac{3}{8}u_P - \frac{1}{8}u_{EE}\right)[[-F_e, 0]]. \tag{10}$$

The v-momentum equation has been discretized in a similar manner.

The governing discretized equations are solved through a pressure correction algorithm, SIMPLE [28]. The pressure link between the continuity and momentum equations is accomplished by transforming the discretized continuity equation into a Poisson equation for pressure correction. This Poisson equation implements a pressure correction for a divergent velocity field. The pressure

DOI: 10.1002/fld

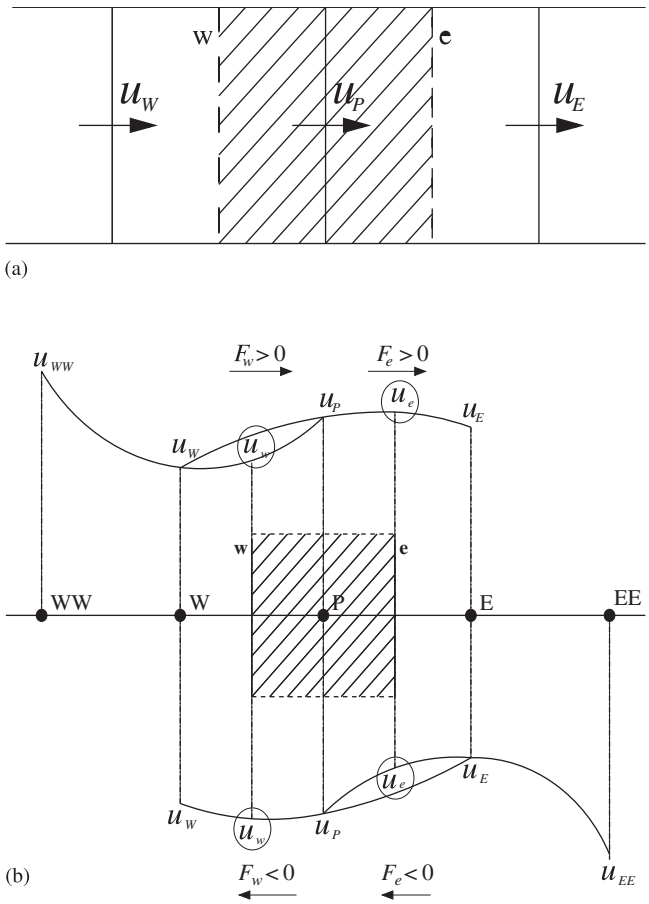

Figure 2. Schematic diagram of (a) u-control volume and (b) quadratic upstream-based interpolation for u.

Poisson equation is given by

$$\frac{p'_{i+1,j}-2p'_{i,j}+p'_{i-1,j}}{\delta r_i^2}+\frac{p'_{i+1,j}-p'_{i,j}}{r_i\delta r_i}+\frac{p'_{i,j+1}-2p'_{i,j}+p'_{i,j-1}}{r_i^2\delta\theta^2}$$
$$=\frac{1}{\delta t}\left[\frac{u^c_{i,j}-u^c_{i-1,j}}{\delta r_i}+\frac{u^c_{i,j}}{r_i}+\frac{v^c_{i,j}-v^c_{i,j-1}}{r_i\delta\theta}\right].$$

The variable p' denotes the pressure correction, and u^c and v^c denote the velocity components obtained by solving the momentum equations. Thus at any time step, a single iteration in this algorithm consists of the following sequential steps:

1. An implicit calculation of the momentum equations is performed. The equations are discretized through the scheme as discussed above. Owing to the coupling of the momentum equations, we solved the system of algebraic equations through a block elimination method [29].
2. The Poisson equation for pressure correction is solved using the successive under relaxation method.
3. The velocity field at each cell is updated using the pressure correction.

Iteration at each time step is continued until divergence-free velocity field is obtained. However, for this purpose, the divergence in each cell is towed below a preassigned small quantity, $\varepsilon=0.5\times10^4$.

A sharp change of thermo-physical properties, such as the permeability, porosity, etc. occurs along the fluid–porous interface. A harmonic mean formulation is used to handle such jump of

DOI: 10.1002/fld

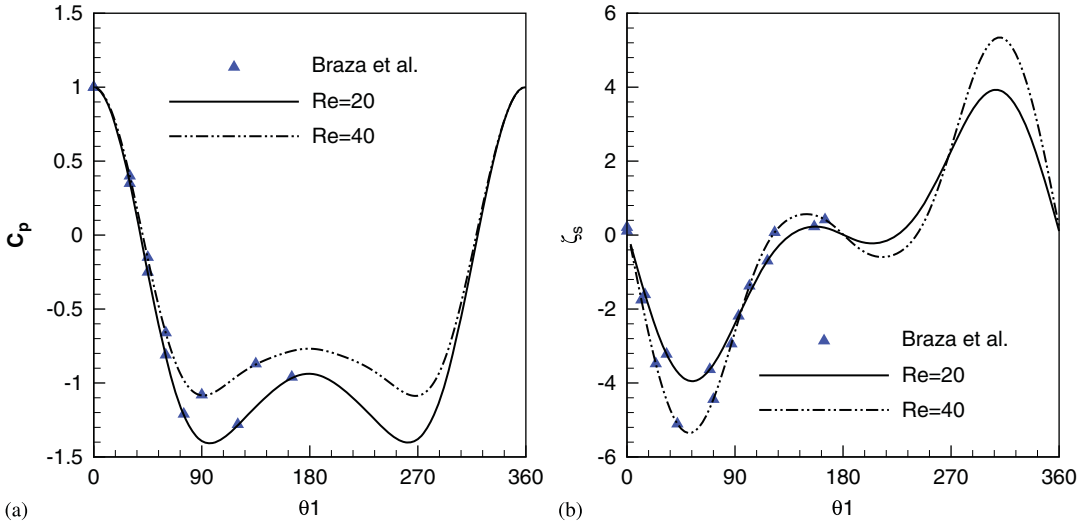

Figure 3. Comparison of (a) surface pressure coefficient ($C_p = (p_s^* - p_o^* + 0.5\rho U_\infty^2)/0.5\rho U_\infty^2$); (b) surface vorticity ($\zeta_s = \zeta R/U_\infty$) with Braza *et al.* [30] for forced convection at different $Re(=20, 40)$ when no porous layer is considered ($e_p = 0$).

the parameter values. As the velocity field along the solid–porous interface and the fluid–porous interface varies more rapidly than elsewhere, a non-uniform grid distribution along the r-direction and uniform grid distribution along θ-direction is incorporated into the computation domain. We made a grid independence study by considering three sets of non-uniform grids, namely 460×290, 400×260, and 300×224, with the first and second number being the total number of grid points in the θ and r-direction, respectively. For the coarse grid, the minimum value of grid size is along r-direction, i.e. $\delta r = 0.01$, whereas for the dense grid $\delta r = 0.005$. The $\delta\theta$ value is taken to be 0.02095 for coarse grid and 0.01366 for dense grid. We compared the values of the drag coefficient obtained by the above set of grids and found that at $Re = 40$, for example the maximum percentage difference between the grids 460×290 and 400×260 is 0.76. The maximum percentage difference between 460×290 and 300×224 is 2.243. We find from the grid independence study that the grids 400×260 is optimal. The outer boundary for the present computation is placed at $20R$ from the center of the cylinder at $Re = 40$. This distance is varied with the variation of Reynolds number.

In the present study, the computations are started either from rest or from the converged solution relating to lower Reynolds number. The time step is taken to be 0.001. After a short transition state, the flow either approaches a steady state or an unsteady time-periodic, depending on the Reynolds number and other flow parameters. The steady flow or the time periodic flow is independent of the initial conditions for the present range of Reynolds number.

To check the validity of our numerical method, we have compared (Figure 3) surface pressure coefficient (relative to the front stagnation point pressure p_o) and surface vorticity (ζ_s) when $Re = 20, 40$ for the case of without porous layer ($e_p = 0$) with those of Braza *et al.* [30]. Figure 4(a),(b) shows the comparisons of our computed Strouhal number (St) and drag coefficient ($\overline{C_d}$) at different Reynolds numbers for $e_p = 0$ case with the experimental/numerical results due to Williamson [22] and Baranyi [31]. Figures 3 and 4 show that our results are in excellent agreement with those of the above published results.

4. RESULTS AND DISCUSSION

The flow field is governed by physical parameters, such as Darcy number (Da), porosity (ε), Reynolds number (Re), and the geometrical parameter e_p, which measures the non-dimensional thickness of the porous layer. We carried out a parametric study in which we fixed the fluid

DOI: 10.1002/fld

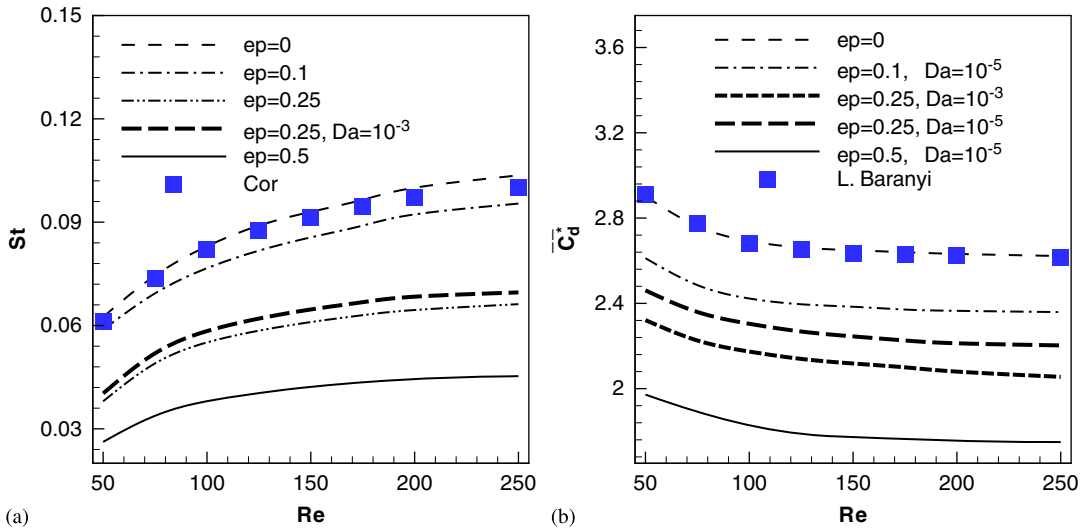

Figure 4. Variation of Strouhal number (St) and period-averaged normalized drag coefficient ($\overline{C_d^*}$) with Re at different e_p. Comparison of our computed St with correlation (Equation (11)) and $\overline{C_d^*}$ with the results due to Baranyi [31] for $e_p = 0$ (solid cylinder) is also included. (a) Strouhal number; (b) period average normalized drag coefficient. In all the other cases $Da = 10^{-5}$.

properties, such as viscosity, density and varied the permeability, porosity, and the porous layer thickness. The flow field is considered for different values of porous layer thickness (e_p) for moderate range of Re, i.e. $40 \leqslant Re \leqslant 200$. We consider that the porous layer consists of foam materials with high porosity ($\varepsilon \geqslant 0.9$, [7]). The Darcy number is assumed to vary between 10^{-2} and 10^{-5}. We inferred that the variation in ε within the range of Da and Re considered here does not produce any significant change in the solution, and hence we present results for $\varepsilon = 0.9$.

4.1. *Control of wake flow*

When a bluff body (non-streamlined) is placed in a uniform stream of fluid, two separated shear layers are formed, one on each side of the body, the vorticity of the two layers being opposite. For the case of a solid cylinder wrapped with a porous layer, the strength of the separated shear layers is reduced. For a solid cylinder, the vorticity diffuses from the surface into the external flow field, whereas vorticity diffuses into both the external and internal flow fields when a porous layer is considered. The critical value of the Reynolds number for the onset of vortex shedding increases with the increase in porous layer thickness. Figure 5 shows an estimate of the critical Reynolds number as a function of the porous layer thickness at different values of permeability (i.e. Da). Beyond this critical Reynolds number, the flow becomes periodic. We find that an introduction of a thin porous wrapper delays the vortex shedding substantially. The increment in critical Re with the increase of e_p is fast in the lower range of e_p (< 0.5). The critical Reynolds number for the onset of vortex shedding is higher with the reduction in porous layer permeability (k). If the porous-wrapped cylinder is replaced by a rigid cylinder of equivalent radius, then the effective Reynolds number is $Re(1+e_p)$. We find from the results that even at $Da = 10^{-5}$, the critical Re is much lower than $40(1+e_p)$, which is the corresponding Re for an equivalent rigid cylinder.

The time dependency of the velocity field inside and outside the porous layer is depicted in Figure 6(a),(b). The control points are located at $r = 1+e_p+0.1$ and $r = 1+e_p-0.1$ on the central axis ($y = 0$) with $e_p = 0.5$. The fluid velocity inside the porous zone is small and temporal fluctuation of velocity field within the porous region occurs at a much lower frequency compared with the fluid outside the porous region. Bruneau and Mortazavi [11, 13] also observed that the wake flow become regularized due to the inclusion of the porous wrapper.

DOI: 10.1002/fld

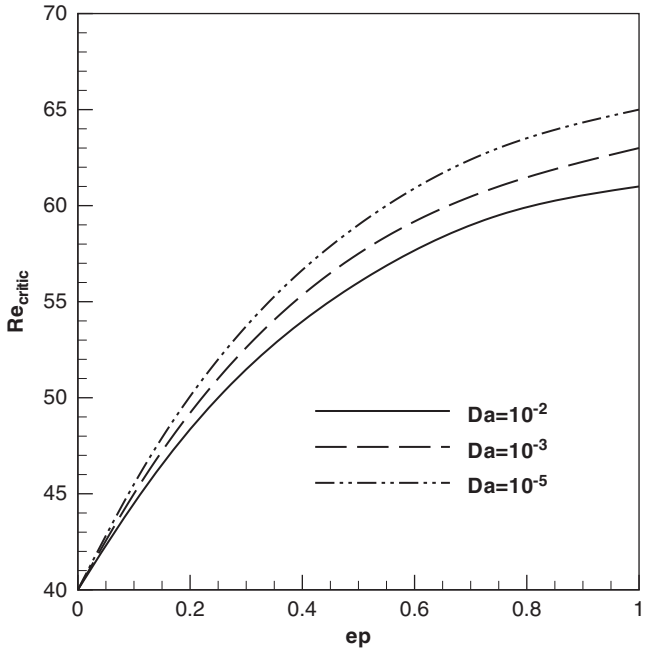

Figure 5. Critical Reynolds number at which vortex shedding start for different porous layer thicknesses.

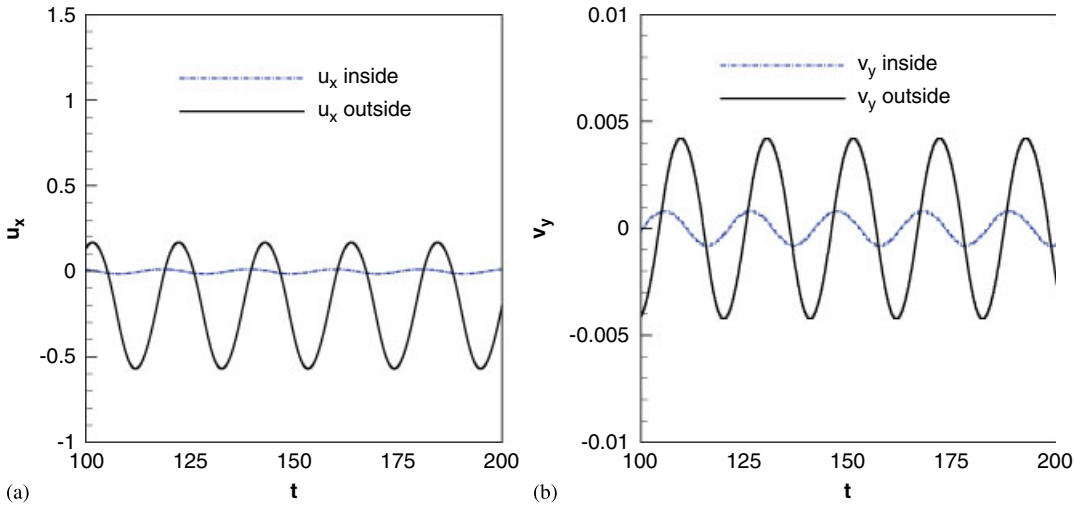

Figure 6. Time evolution of Cartesian velocities component: (a) x-component (u_x) and (b) y-component (v_y) for $Re=200$ and $Da=10^{-5}$.

Along the outer surface of the bluff body, boundary layers of slow-moving viscous fluids are formed and, because it is not streamlined and the fluid flow cannot follow the contours of the body, it becomes detached and rolls up into vortices. For the case of a solid cylinder ($e_p=0$) when Reynolds number is beyond 40, the shear layers exhibit Kelvin–Helmeholtz instability and an alternate vortex shedding is observed. The time-periodic flow behind the cylinder is demonstrated with the aid of instantaneous vorticity contours during a complete vortex shedding cycle. The results are shown in Figure 7(a)–(d) at Reynolds number 200 and $e_p=0.5$. The Darcy number for the porous layer is considered to be $Da=10^{-5}$. The time period T_p for the vortex shedding cycle is the difference between the two successive non-dimensional times at which the lift

DOI: 10.1002/fld

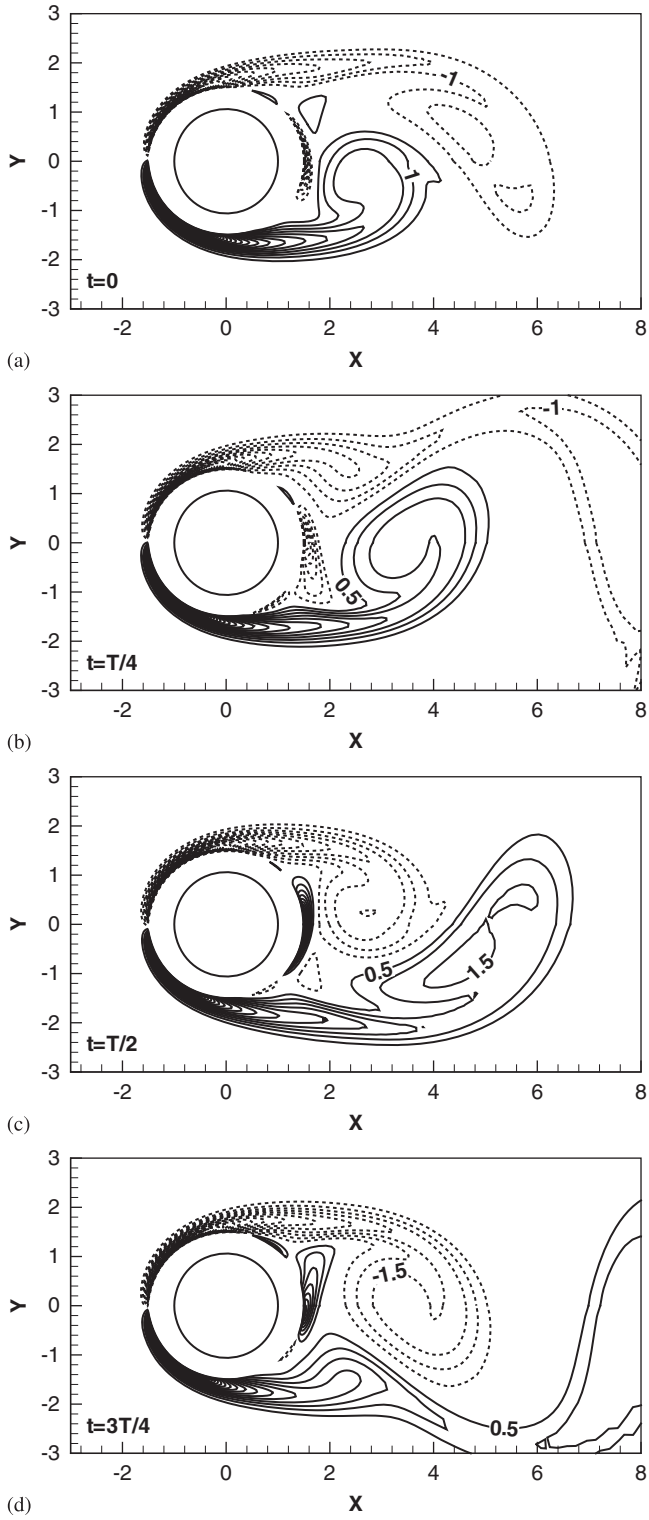

(a)

(b)

(c)

(d)

Figure 7. Vorticity contours (a)–(d) during one shedding for $Re = 200$, $e_p = 0.5$ and $Da = 10^{-5}$.

DOI: 10.1002/fld

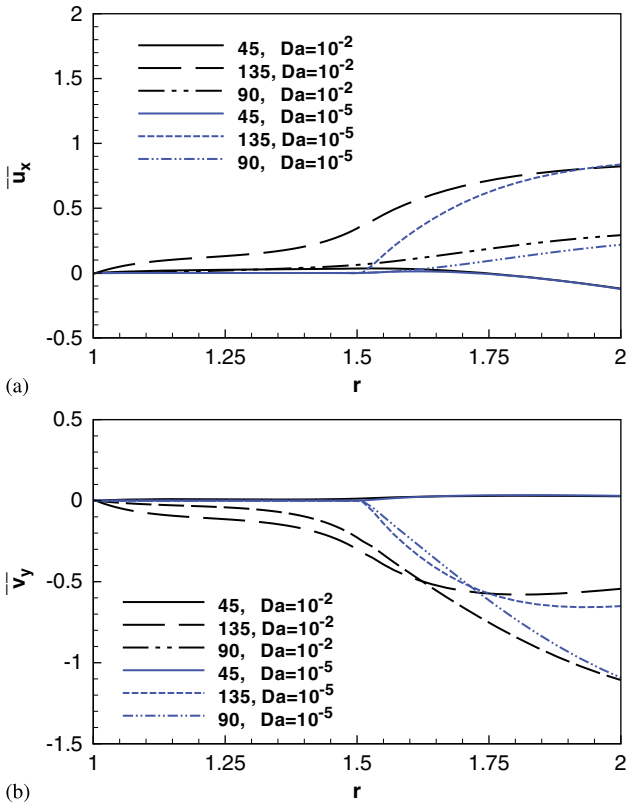

Figure 8. Period-averaged Cartesian velocity component: (a) x-component (u_x) and (b) y-component (v_y) along radial distance r for different $\theta(=45, 90, 135)$ at $e_p=0.5$ when $Re=200$ and $Da=10^{-5}$.

coefficient attains its minimum value. The non-dimensional shedding period (T_p) is found to be 22.47 for the present set of parameter values. The fluid penetration inside the porous layer is almost negligible at this lower value of permeability, thus the outer surface of the porous layer behaves like a solid body and deflects most of the approaching fluid. Vortex sheds from the separated shear layers emerging from the outer surface of the porous layer. The part of the vorticity of the separated shear layer is diffused along the inner side of the porous layer, thus the strength of the shear layers is weaker compared with the case when the solid cylinder is considered ($e_p=0$).

The vorticity contours (Figure 7(a)–(d)) show that the fluid–porous interface can be interpreted to consist of two layers, one the pseudo-boundary layer inside the fluid zone and other the thin layer inside the porous region. At the fluid–porous interface, there is effectively a slip velocity on the porous surface and the boundary layer which develops above the porous layer is different from the classical Prandtl boundary layer. Within the interface region inside the porous zone, the velocity evolves from the Darcy velocity to the interface velocity with a growth of $O(\sqrt{k})$ [11, 32]. In addition, there exists a boundary layer adjacent to the porous–solid interface. Based on an analysis of infinite porous medium over a solid boundary, Vafai and Tien [33] observed that the boundary effect is confined to a very thin momentum boundary layer and often plays an insignificant role in overall flow consideration. The period-averaged Cartesian components of velocity profiles at different θ-positions are presented in Figure 8(a),(b) at different values of $Da=10^{-2}$, 10^{-5} for $Re=200$ and $e_p=0.5$. It is evident from the results that the flow field strictly depends on the Reynolds number where both the spatial gradient is strong. Thus, an analysis based on boundary layer assumption may not be valid in this case. We also found that the growth of the velocity field within the porous zone is faster at higher Da.

DOI: 10.1002/fld

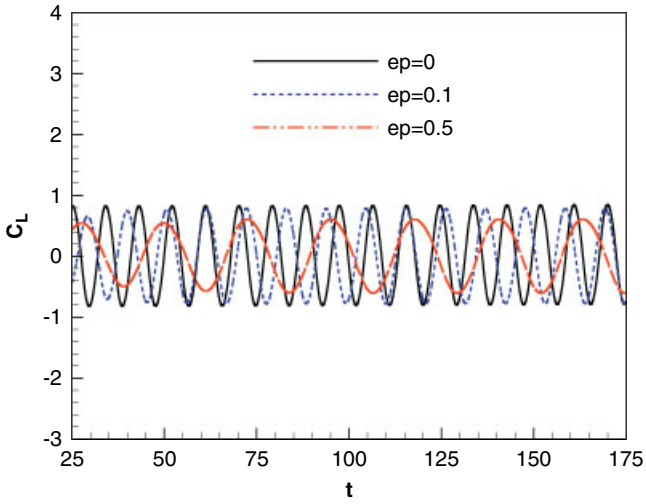

Figure 9. Time evolution of lift coefficient (C_L) when $Re=200$ for different e_p at $Da=10^{-5}$.

4.2. *Strouhal number and drag coefficient*

In Figure 9, we have presented the time evolution of the lift coefficient for $Re=200$ and $Da=10^{-5}$ at different values of the porous layer thickness (e_p). It shows that the amplitude of oscillation of C_L is decreased with the increase of e_p. We find that the time average lift experienced by the cylinder is close to zero, when the flow remains symmetric.

The Strouhal number (St) measures the vortex shedding frequency and is obtained through the frequency of oscillation of the lift coefficient for the solid cylinder. The variation in St with Re at different e_p is shown in Figure 4(a). A steep jump in St from the corresponding solid cylinder case ($e_p=0$) is observed with the introduction of the porous wrapper. The St also depends strongly on the permeability of the porous medium. Through experimental study (for $e_p=0$ case), Williamson [22] proposed the correlation between St and Re as follows:

$$St=\frac{A}{Re}+B+C\,Re, \tag{11}$$

where $A=-3.3265$, $B=0.1816$, and $C=1.6\times10^{-4}$. Our numerical results (Figure 4(a)) for $e_p=0$ is in good agreement with the above correlation. The St versus Re curves in Figure 4(a) indicate that the variation of Strouhal number with Re is almost similar at different e_p and the trend in St–Re variation is similar to the above correlation.

The variation of time-averaged surface pressure ($\overline{C_p}$) along the solid cylinder and the fluid–porous interface is presented in Figure 10(a),(b) for different values of the porous layer thickness at $Re=200$. The sliding of separation points toward the upstream with the inclusion of a porous wrapper is evident from the location of pressure minima. The pressure suction is reduced, but the base pressure is increased with the inclusion of the porous wrapper. The higher base pressure results in lower drag coefficient. The pressure variation along the interface is almost similar to that of the variation of pressure along the solid cylinder.

The dependence of time-averaged normalized drag coefficient of the porous-sheathed cylinder on the Reynolds number is illustrated in Figure 4(b) at different values of the porous layer thickness of different permeabilities. Here we have scaled the drag coefficient by $(1+e_p)$, i.e. $\overline{C_d^*}=\overline{C_d}/(1+e_p)$, in order to compare the drag of equal radius. Thus, $\overline{C_d^*}$ is the drag coefficient for the cylindrical structure of radius R consisting of a inner solid cylinder wrapped by a porous layer. The drag experienced by a bluff structure is composed of two parts: frictional drag and pressure drag. The skin friction along the fluid–porous interface is much reduced compared with the solid–fluid interface as the vorticity strength is lower in the former case. Besides, the pressure drop along

DOI: 10.1002/fld

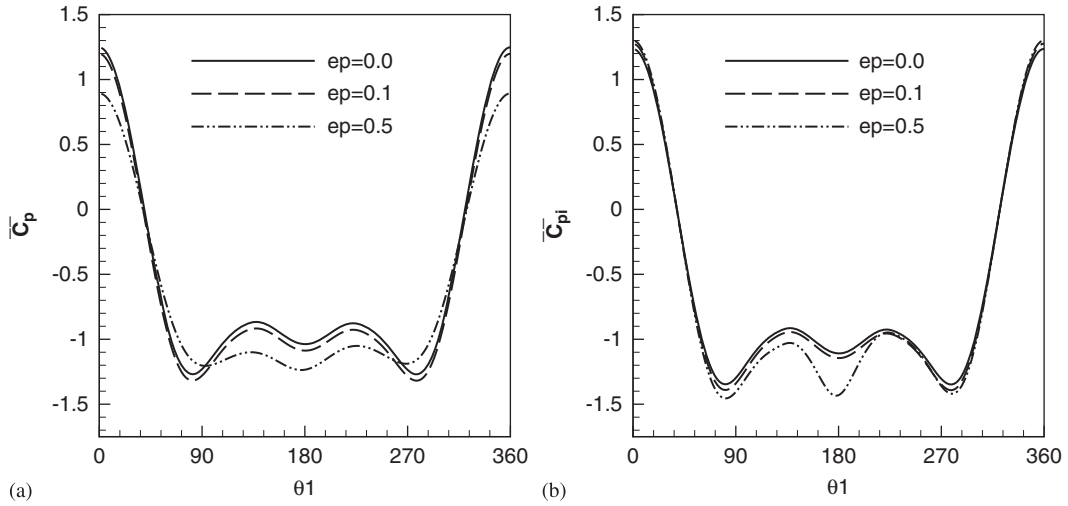

Figure 10. Distribution of the period-averaged surface pressure coefficient: (a) along solid surface ($\overline{C_p}$) and (b) along interface ($\overline{C_{pi}}$) at different thickness of porous layer when $Re=200$ and $Da=10^{-5}$.

the fluid–porous interface is also lower compared with a solid–fluid interface at a fixed Reynolds number. Thus, the total drag experienced by a porous-wrapped solid cylinder will be lower than a solid cylinder of equal radius. Figure 4(a),(b) shows that the variation of St and $\overline{C_d}$ with Re at different e_p are almost similar. The order of drag reduction must vary with the permeability of the porous material. By varying Da, we found that the increase in permeability of the porous layer produces reduction in drag coefficient.

4.2.1. Effect of porous layer thickness and permeability. In order to investigate the damping effect of a porous sheath, we present St as a function of the porous layer thickness at different Re (Figure 11(a)). The increase in porous layer thickness produces a large damping effect on the vortex shedding frequency. We find from the results that the reduction in St with the increment of e_p is much faster when $e_p<0.5$. The Strouhal number approaches zero asymptotically, i.e. a steady flow develops at sufficiently large value of e_p.

Figure 11(b) shows the frequency factor H, which measures the ratio of St obtained for non-zero e_p with St due to a solid cylinder, as a function of Re at different values of the porous layer thickness. We have also varied the permeability (i.e. Da) of the porous layer in investigating the effect on the frequency of vibration. A significant reduction in shedding frequency through the introduction of porous wrapper is evident from this result. The frequency ratio assumes almost a constant value, i.e. independent of Reynolds number when $Re\geqslant 80$. This indicates that the variation of St with Re for porous-wrapped solid cylinder is similar to the case of $e_p=0$. The flow within the porous layer is almost linear, hence the vibration frequency of the porous-wrapped cylinder is damped but follow the similar pattern as that of the solid structure. With the increase in the Darcy number at a fixed Re and e_p, the frequency factor increases. As the porous layer is more permeable the velocity of the fluid approaching the cylinder is higher, and hence the frequency of vortex shedding is enhanced compared with the case of lower permeability. For a higher permeable porous medium or turbulent flow (large Re), the convection effect in the porous layer may become prominent. We have seen in Figure 5 that at a fixed e_p, the increase in permeability of the porous layer reduces the critical value of Re for the onset of vortex shedding.

The dependence of time-averaged drag coefficient $\overline{C_d}$ on the porous layer thickness at different values of Reynolds number is depicted in Figure 12(a). Here we have varied the porous layer thickness up to four times the radius of the solid cylinder. Drag increases with the increase in surface area and reduces with the increase in Re. However, it is evident from Figure 12(a) that $\overline{C_d}$ of a porous-wrapped cylinder is lower when compared with a solid cylinder of equal radius.

DOI: 10.1002/fld

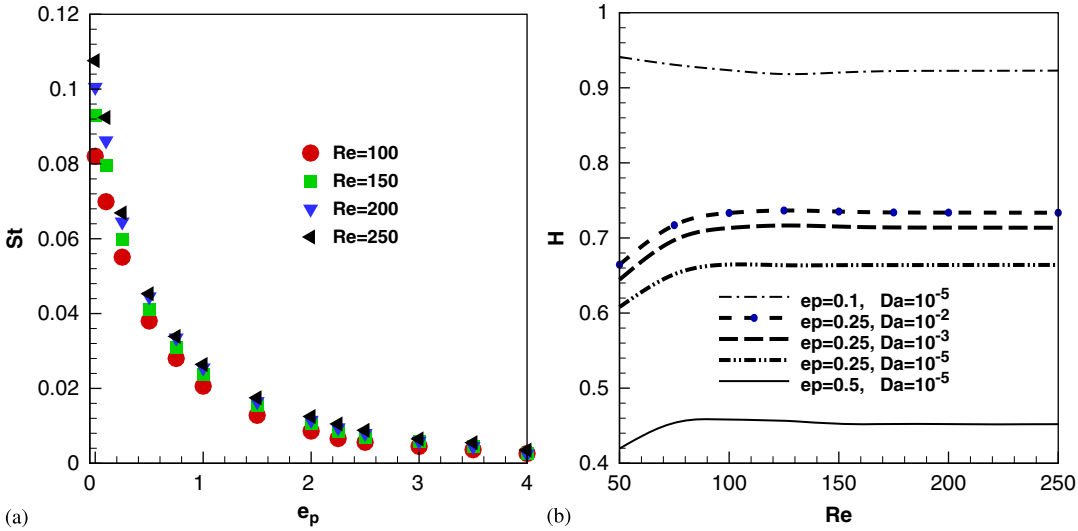

Figure 11. Variation of Strouhal number (St) and Strouhal number ratio ($H = St/(St)_{\text{solid}}$) with e_p and Re: (a) St with e_p at different Re with $Da = 10^{-5}$ and (b) H versus Re at different e_p.

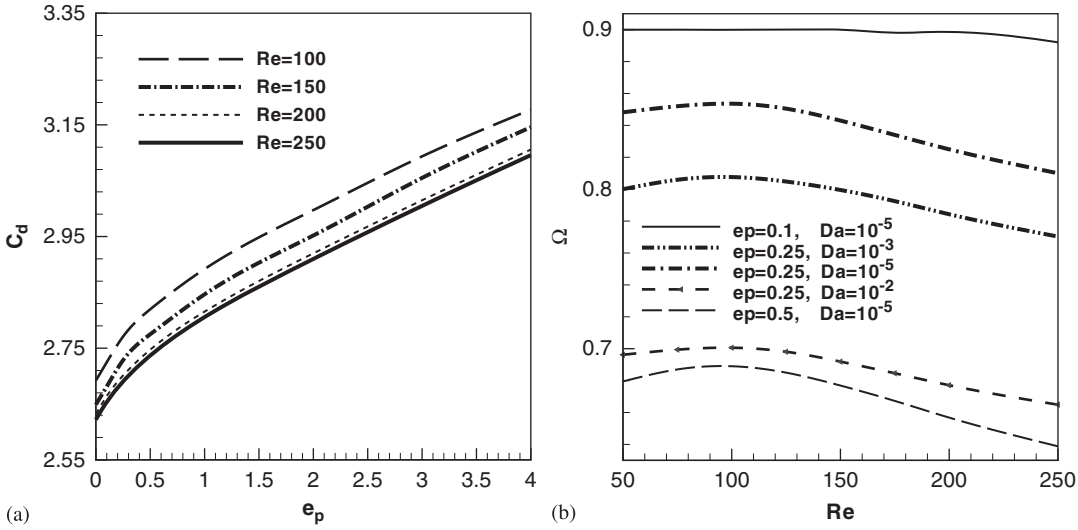

Figure 12. Variation of period-averaged drag coefficient ($\overline{C_{\text{d}}}$) and drag factor ($\Omega = \overline{C_d^*}/(\overline{C_{\text{d}}})_{\text{solid}}$) with e_p and Re at $Da = 10^{-5}$: (a) $\overline{C_{\text{d}}}$ with e_p at different Re and (b) Ω with Re at different e_p.

For example, the $\overline{C_{\text{d}}}$ of a solid cylinder of radius 1.5 at $Re = 250$ can be estimated as 3.93, which is higher compared with a porous-sheathed cylinder of radius 1.5. We find that the variation of $\overline{C_{\text{d}}}$ with e_p is similar for all the Re presented here.

The drag factor, $\Omega = \overline{C_{\text{d}}^*}/(\overline{C_{\text{d}}})_{\text{solid}}$, which is the ratio of the normalized drag with the corresponding solid drag ($e_p = 0$), is presented as a function of Re at different e_p in Figure 12(b). We have also varied the permeability of the porous medium, i.e. $Da = 10^{-2}$ to 10^{-5}. A significant drag reduction through the inclusion of porous wrapper is evident from this result. As the porous layer becomes more permeable, resistance experienced by the fluid in passing through the porous layer is less and thus the drag experienced by the porous-wrapped cylinder is lower. The result shows that a thin porous wrapper of thickness 0.1 times the radius of the cylinder produces drag reduction about 8.45% when $Re = 100$, 8.30% when $Re = 150$, and 8.20% drag reduction when

DOI: 10.1002/fld

$Re=200$. For $e_p=0.5$, the maximum percentage of drag reduction is about 32.34% when $Re=50$. Figure 12(b) provides a guideline for optimal value of the porous layer thickness to construct a structure composed of inner solid body of radius $R/(1+e_p)$ and a porous sheath of thickness $Re_p/(1+e_p)$ so as to have a drag reduction of desired order. We find that increase in porous layer thickness produces a substantial drag reduction at a fixed value of the permeability. The drag on the composite structure can be reduced also by increasing the permeability at a fixed e_p.

5. CONCLUSION

The laminar vortex shedding behind a porous-wrapped solid cylinder is investigated for Reynolds number up to 250. The flow remains symmetric about the central line for this range of Reynolds number and hence the average lift coefficient is found to be zero. Inclusion of a porous wrapper weakens the strength of the separated shear layers and hence delays the vortex shedding. The porous wrapper reduces the pressure drop and skin friction which leads to a reduction in drag compared with a solid cylinder of equal radius. The wake characteristics are similar to that of a wake due to a solid cylinder when a thin porous wrapper ($e_p<1$) is considered. At large values of e_p, which depends on Re and Da, the flow field approaches to steady state. The temporal fluctuation of velocity components inside the porous region is found to be significantly damped. The nonlinear effects are negligible inside the porous zone and therefore the variation of porosity at a fixed value of permeability has no significant effect. The St–Re and $\overline{C_d^*}$–Re curves show similar trends at different values of the porous layer thickness.

The critical value of Reynolds number, for the onset of vortex shedding, increases almost linearly with the increase in porous layer thickness. This critical value of Re strongly depends on the permeability of the porous medium. With the decrease in permeability the resistance to fluid flow in the porous zone increases, which gives rise to an increment in drag coefficient and reduction in Strouhal number. The inclusion of a porous wrapper produces significant damping effect on the vortex-induced oscillation of the solid cylinder and St decreases monotonically as e_p increases. We found that a thinner porous layer of lower Da has an equivalent effect of a thicker porous layer of higher permeability. Our computed results may provide a guideline in constructing the composite structure to have an optimal vortex-induced vibration and drag force.

ACKNOWLEDGEMENTS

We acknowledge the financial support received from the Council of Scientific & Industrial Research, India through a research project grant. We sincerely thank the referees for their valuable comments.

REFERENCES

1. Owen JC, Bearman PW, Szewczyk AA. Passive control of VIV with drag reduction. *Journal of Fluids and Structures* 2000; **115**:597–605.
2. Roshko A. On the wake and drag of bluff bodies. *Journal of Aeronautical Science* 1955; **22**:124–132.
3. Ozono S. Flow control of vortex shedding by a short splitter plate asymmetrically arranged downstream of a cylinder. *Physics of Fluids* 1999; **10**:2928–2934.
4. Ozono S. Vortex suppression of the cylinder wake by deflectors. *Journal of Wind Engineering and Industrial Aerodynamics* 2003; **91**:91–99.
5. Hwang JY, Yang KS, Sun SH. Reduction of flow-induced forces on circular cylinder using a detached splitter plate. *Physics of Fluids* 2003; **15**:2433–2436.
6. Nakamura H, Igarshi T. Omnidirectional reductions in drag and fluctuating forces for a circular cylinder by attaching rings. *Journal of Wind Engineering and Industrial Aerodynamics* 2008; **96**:887.
7. Phanikumar MS, Mahajan RL. Non-Darcy natural convection in high porosity metal foams. *International Journal of Heat and Mass Transfer* 2002; **45**:3781–3793.
8. Vafai K, Kim SJ. Analysis of surface enhancement by porous substrate. *Journal of Heat Transfer* 1990; **112**: 700–705.
9. Srinivasan KR, Loth E, Dutton JC. Aerodynamics of recirculating flow control devices for normal shock/boundary-layer interactions. *AIAA Journal* 2006; **44**:751–763.

DOI: 10.1002/fld

10. Bruneau CH, Mortazavi I. Passive control of the flow around a square cylinder using porous media. *International Journal for Numerical Methods of Fluids* 2004; **46**:415–433.
11. Bruneau CH, Mortazavi I. Control of vortex shedding around a pipe section using a porous sheath. *International Journal of Offshore and Polar Engineering* 2006; **16**:90–96.
12. Bruneau CH, Mortazavi I, Gillieron P. Passive control around the two-dimensional square back Ahmed body using porous devices. *Journal of Fluids Engineering* 2008; **130**:61–101.
13. Bruneau CH, Mortazavi I. Numerical modeling and passive flow control using porous media. *Computers and Fluids* 2008; **37**:488–498.
14. Sobera MP, Kleijn CR, Van den Akker HEA. Subcritical flow past a circular cylinder surrounded by a porous layer. *Physics of Fluids* 2006; **18**:38–106.
15. Ingham DB, Pop I (eds). *Transport Phenomena in Porous Media*, vol. 3. Elsevier: Oxford, 2005; 751–763.
16. Nazar R, Amin N, Filip D, Pop I. The Brinkman model for the mixed convection boundary layer flow past a horizontal circular cylinder in a porous medium. *International Journal of Heat and Mass Transfer* 2003; **46**:3167–3178.
17. Khanafer K, Amiri AA, Pop I. Numerical analysis of natural convection heat transfer in a horizontal annulus partially filled with a fluid-saturated porous substrate. *International Journal of Heat and Mass Transfer* 2008; **51**:1613–1627.
18. Costa UMS, Andrade Jr JS, Makse HA, Stanley HK. The role of inertia on fluid flow through disordered porous media. *Physics A* 1999; **266**:420.
19. Fourar M, Radilla G, Lenormand R, Moyne C. On the non-linear behavior of a laminar single-phase flow through two and three-dimensional porous media. *Advances in Water Resources* 2004; **27**:669.
20. Beavers GS, Joseph DD. Boundary condition at a naturally permeable wall. *Journal of Fluid Mechanics* 1967; **30**:197–207.
21. Saffman P. On the boundary condition at the interface of a porous medium. *Studies Applied Mathematics* 1971; **50**:93–101.
22. Williamson CHK. Oblique and parallel modes of vortex shedding in the wake of a circular cylinder at low Reynolds numbers. *Journal of Fluid Mechanics* 1989; **206**:579–627.
23. Hammache M, Gharib M. An experimental study of the parallel and oblique vortex shedding from circular cylinders. *Journal of Fluid Mechanics* 1991; **232**:567–590.
24. Perry AE, Chong MS, Lim TT. The vortex-shedding process behind two-dimensional bluff bodies. *Journal of Fluid Mechanics* 1982; **116**:77–90.
25. Nield A, Bejan A. *Convective Heat Transfer in Porous Media*. Springer: New York, NY, 1998.
26. Vafai K. Convective flow and heat transfer in variable-porosity media. *Journal of Fluid Mechanics* 1984; **147**:233–259.
27. Bhattacharyya S, Dhinakaran S, Khalili A. Fluid motion around and through a porous cylinder. *Chemical Engineering Science* 2006; **61**:4451–4461.
28. Fletcher CAJ. *Computation Technique for Fluid Dynamics*, vol. 2. Springer: Berlin, 1998.
29. Varga RS. *Matrix Iterative Analysis*. Prentice-Hall: Englewood Cliffs, NJ, 1962.
30. Braza M, Chassaing P, Ha Minh H. Numerical study and physical analysis of the pressure and velocity field in the near wake of a circular cylinder. *Journal of Fluid Mechanics* 1986; **165**:79–130.
31. Baranyi L. Computation of unsteady momentum and heat transfer from a fixed circular cylinder in laminar flow. *Journal of Computational Applied Mechanics* 2003; **4**:13–25.
32. Breugem WP, Boersma BJ, Uittenbogaard RE. The laminar boundary layer over a permeable wall. *Transport in Porous Media* 2005; **59**:267–300.
33. Vafai K, Tien CL. Boundary and inertia effects on flow and heat transfer in porous media. *International Journal of Heat Mass Transfer* 1981; **24**:195–203.

DOI: 10.1002/fld